Continental Shelf Research 117 (2016) 12–19

Contents lists available at ScienceDirect

Continental Shelf Research

journal homepage: www.elsevier.com/locate/csr

Research papers

Observational evidence for tidal straining over a sloping continental shelf

Takahiro Endoh [a,*], Yutaka Yoshikawa [b], Takeshi Matsuno [c], Yoshinobu Wakata [c], Keun-Jong Lee [d], Lars Umlauf [e]

[a] UTokyo Ocean Alliance, The University of Tokyo, Tokyo, Japan
[b] Division of Earth and Planetary Sciences, Graduate School of Science, Kyoto University, Kyoto, Japan
[c] Research Institute for Applied Mechanics, Kyushu University, Fukuoka, Japan
[d] Interdiciplinary Graduate School of Engineering Sciences, Kyushu University, Fukuoka, Japan
[e] Leibniz-Institute for Baltic Sea Research Warnemünde, Warnemünde, Germany

ARTICLE INFO

Article history:
Received 6 July 2015
Received in revised form
28 January 2016
Accepted 29 January 2016
Available online 30 January 2016

Keywords:
Bottom boundary layer (BBL)
Tidal straining
Tidally-periodic stratification
Shear-induced convection
Microstructure profiler
Acoustic Doppler current profiler

ABSTRACT

Straining of a horizontal density gradient by tidal currents acts to periodically produce and destroy near-bottom stratification, which has been shown to modulate turbulence in the bottom boundary layer (BBL). Previous observations of such periodic variations have been limited to the coastal ocean and estuaries, where horizontal density gradients are maintained by river runoff or differential heating. In the present study, we show evidence for the existence of tidal straining over the continental shelf, outside any regions of freshwater influence, where horizontal density gradients are likely to result from the projection of the interior vertical stratification onto sloping topography. Based on microstructure data obtained in the East China Sea, we demonstrate that the tidal current shear interacting with the cross-isobath density gradient results in semidiurnal switching between unstable and stable stratification in the lower part of the BBL. The cycle of turbulent dissipation is quarter-diurnal, corresponding to the semidiurnal variation of tidal current shear. In addition, a noticeable diurnal modulation in stratification as well as a significant diurnal cycle of turbulent dissipation are observed in the upper part of the BBL, where the time evolution of stratification is dominated by tidal advection, rather than tidal straining.

1. Introduction

On the continental shelf and in the coastal ocean, turbulent mixing in the bottom boundary layer (BBL) is one of the key mechanisms for the dissipation of kinetic energy, for the transport of scalars such as heat, salt, nutrients, and sediment, and for the fluxes across the sediment–water interface. In the BBL, where the current speed is reduced to zero towards the bottom due to friction, straining of a horizontal density gradient acts both to produce and destroy stratification during the tidal cycle. This process, often referred to as "tidal straining", is known to trigger periodic modulations of near-bottom turbulence with some important implications for mixing and residual transports inside the BBL. The cycling between unstable and stable stratification induced by tidal straining is often called "Strain-Induced Periodic Stratification (SIPS)" (Simpson et al., 1990), which has been so far observed mainly in the coastal ocean (Simpson and Souza, 1995; Rippeth et al., 2001; Fisher et al., 2002) as well as in estuaries (Nepf and Geyer, 1996; Stacey et al., 1999a). A necessary prerequisite for the existence of SIPS is a background horizontal density gradient, typically maintained by river runoff in a "Region of Freshwater Influence" (ROFI) (Simpson, 1997), or, less frequently, by differential heating of the water column (e.g. Becherer et al., 2015).

Recent observations in lakes and modeling studies, however, suggest an alternative mechanism for the generation of quasi-horizontal density gradients in the vicinity of *sloping* topography, which results in a similar periodic modulation of near-bottom stratification and turbulence. This mechanism is associated with the cross-isobath (i.e. approximately horizontal) density gradient resulting from the projection of the interior vertical stratification onto the slope (see Umlauf and Burchard, 2011, Fig. 1). For the case of a uniform slope with slope angle α and a linear vertical stratification in the interior, i.e. above the strongly turbulent BBL, the cross-isobath (upslope) density gradient is given by $-(\rho_0/g)N_\infty^2 \sin\alpha$, where N_∞ is the buoyancy frequency outside the BBL; g ($=9.81\ \mathrm{ms}^{-2}$) is the acceleration due to gravity; and ρ_0 is the reference density of water (Umlauf and Burchard, 2011). In lakes, the interaction between this cross-isobath density gradient and the

* Corresponding author.
E-mail address: endo@oa.u-tokyo.ac.jp (T. Endoh).

http://dx.doi.org/10.1016/j.csr.2016.01.018
0278-4343/

near-bottom current shear due to internal wave motions has been shown to result in a periodic generation and destruction of near-bottom stratification (Lorke et al. 2005, 2008), which is in many respects similar to SIPS. During periods of upslope flow, deeper, denser water flows on top of less dense water that moves more slowly due to friction, resulting in unstable stratification, and subsequently in "Shear-Induced Convection" (ShIC) (Lorke et al., 2005). Conversely, during periods of downslope flow, less dense, shallower water flows on top of denser water, which enhances stratification in the BBL. Modeling studies have shown that this process occurs over a wide range of parameters and geometries (Umlauf and Burchard, 2011; Becherer and Umlauf, 2011). Although previous observations of the above process have been limited to lakes, a similar behavior is expected to occur wherever an oscillating current shear interacts with horizontal density gradients. In contrast to SIPS, tidal straining over sloping topography requires neither river runoff nor differential heating to create horizontal density gradients, and is therefore likely to occur in much wider areas of the continental shelf. Due to the relatively recent discovery of this process, however, field data supporting the modeling studies mentioned above are so far lacking.

In the present study, we show first observational evidence for the existence of tidal straining over a sloping continental shelf outside any ROFI, using microstructure data obtained in the East China Sea (ECS) in summer. The ECS has a broad continental shelf and slopes with strong tidal currents (Larsen et al., 1985; Yoshikawa et al., 2010), which is favorable for the occurrence of ShIC, and is also known as one of the regions of intense primary productivity. The observations were carried out at about 400 km to the east-northeast of the mouth of the Changjiang River (Fig. 1a), suggesting that the effect of horizontal density gradients maintained by river runoff are negligible or at least of minor importance. The vertical extent of the Changjiang diluted water (CDW), a mixture of the discharged freshwater and the surrounding seawater (Beardsley et al., 1985), is confined to the surface mixed layer near the observation site (Yoshikawa et al., 2012) so that the CDW contributes to maintaining the interior vertical stratification rather than generating horizontal density gradients in the BBL.

In the following sections, we describe field observations and instrumentation (Section 2), followed by our observations of tidally-periodic stratification and mixing in the BBL (Section 3), investigate the roles of semidiurnal and diurnal tidal currents in the time evolution of potential density (Section 4), discuss a difference in the relative importance of tidal straining and advection between the upper and lower parts of the BBL (Section 5), and finally summarize our results (Section 6).

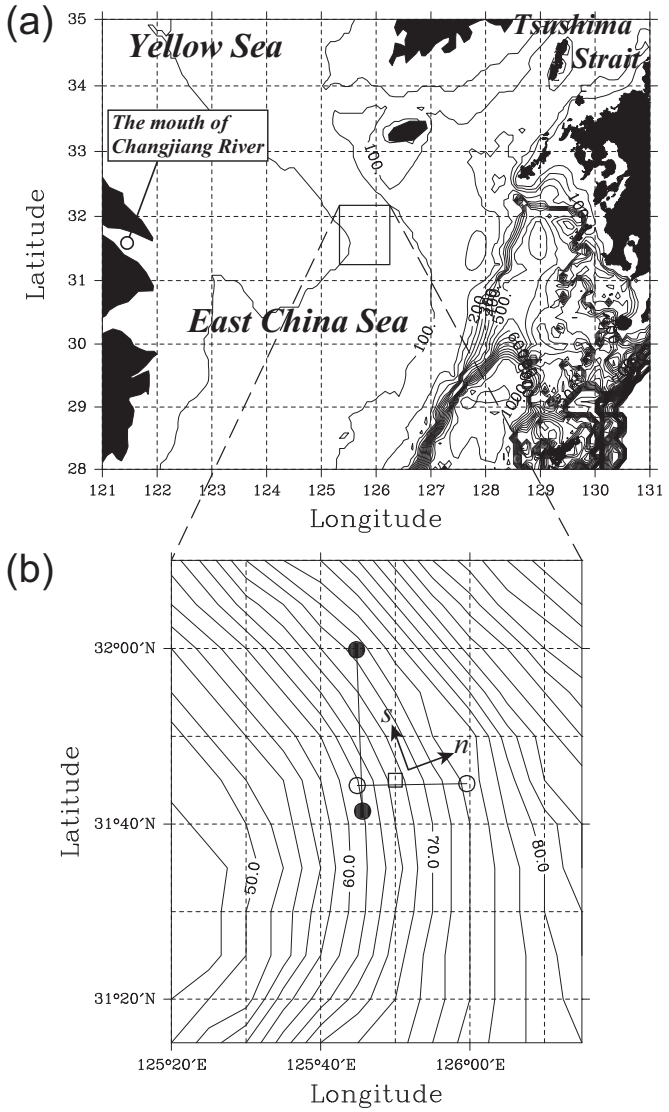

Fig. 1. (a) Map of the East China Sea and (b) an enlargement of the area indicated by the rectangle in panel (a). Bathymetric contours are shown every 50 m and 2 m in panels (a) and (b), respectively. Black shading in panel (a) indicates land. Panel (b) includes the location at which the ADCP and TurboMAP-5 were deployed (open square) as well as the CTD stations used for calculating zonal and meridional gradients of potential density (open and closed circles, respectively). Positive cross-isobath (n) and along-isobath (s) directions are indicated by axes in panel (b). Note that the n-axis points downslope.

2. Observations

The observations were carried out at a position of 31°44.9′N, 125°50.0′E, where the water depth and the inertial period are about 68 m and 23 h, respectively, over the continental shelf of the ECS (Fig. 1) on July 16–21, 2011 during a cruise of the training ship *Nagasaki-Maru* of Nagasaki University. At 1640 JST (Japan Standard Time) on July 16, we deployed an ADCP (Teledyne RD Instruments (RDI), Workhorse 600 kHz) mounted in a trawl-resistant bottom mount in an upward-looking orientation on the seabed composed mostly of muddy sand. The ADCP was operated in the standard RDI "mode 1", sampling and recording the along-beam velocities at 1.3 Hz during 20-min bursts every half hour. The vertical bin size was set to be 1 m, and the depth of the first bin was 65 m, i.e. 3 m above the seabed. In the present study, the ADCP data in the depth range of 30–65 m was used, where the "percentage of good data" (a quality indicator suggested by RDI) was the maximum value of 100 during the entire period of the observations (i.e. all the single-ping data were judged good). From the along-beam velocities averaged over 20 minutes (1600 pings), the cross- and along-isobath components of horizontal velocity (U and V) as well as the zonal and meridional components of horizontal velocity (u and v) were calculated at time intervals of half hour. The cross-isobath (n) and along-isobath (s) directions are indicated in Fig. 1b. The Reynolds stresses estimated by applying the variance method (Lu and Lueck, 1999; Stacey et al., 1999b) directly to the single-ping data were too noisy to be used in the present analysis. Within about 500 m of the ADCP, we deployed a microstructure profiler (JFE Advantech, TurboMAP-5) that samples the micro-scale vertical shear and the micro-scale temperature at a rate of 512 Hz as well as temperature, conductivity, pressure, turbidity, fluorescence, and the acceleration of the instrument at a rate of 64 Hz while falling freely at a speed of 0.5–0.6 ms^{-1} (Wolk et al., 2002). The dissipation rate of turbulent kinetic energy (ε) was calculated from

the micro-scale vertical shear with a sliding window of 1 m, as described in Endoh et al. (2009, 2014). Three profiles from a depth of 10 m down to the seabed were obtained approximately every 1 h between 1700 JST on July 17 and 0600 JST on July 19, which were averaged together to give hourly means. After the microstructure measurements, we took several CTD casts to evaluate horizontal density gradients (on July 19–20), and then recovered the ADCP at 1540 JST on July 21.

3. Tidally-periodic stratification and mixing

Fig. 2 shows that the flow field is dominated by the semidiurnal tide, however, with a significant diurnal modulation that can most clearly be identified during periods of maximum current speed (Fig. 2a and b). The BBL with relatively homogeneous density is confined below a depth of 35 m. There is a clear semidiurnal signal in density variations in the BBL, which is less significant above the BBL.

Overall, the BBL becomes warmer and saltier during periods of upslope flow (negative U), and cooler and fresher during periods of downslope flow (positive U) (Fig. 2a, c and d), reflecting the influence of warm, saline water of the Kuroshio on deeper, denser water, as suggested by Yoshikawa et al. (2012). Maxima (minima) in temperature and salinity follow minima (maxima) in the cross-isobath velocity U with a phase shift of 90°. This result suggests cross-isobath advection as the main cause for the observed variations in temperature and salinity (and hence density), which will be investigated in more detail in the next section.

In the lower part of the BBL (below a depth of 50 m), a semidiurnal switching between unstable ($N^2 < 0$) and stable ($N^2 > 0$) stratification is observed (Fig. 2e), which also lags U with a phase shift of about 90°. The most important feature observed in the lower part

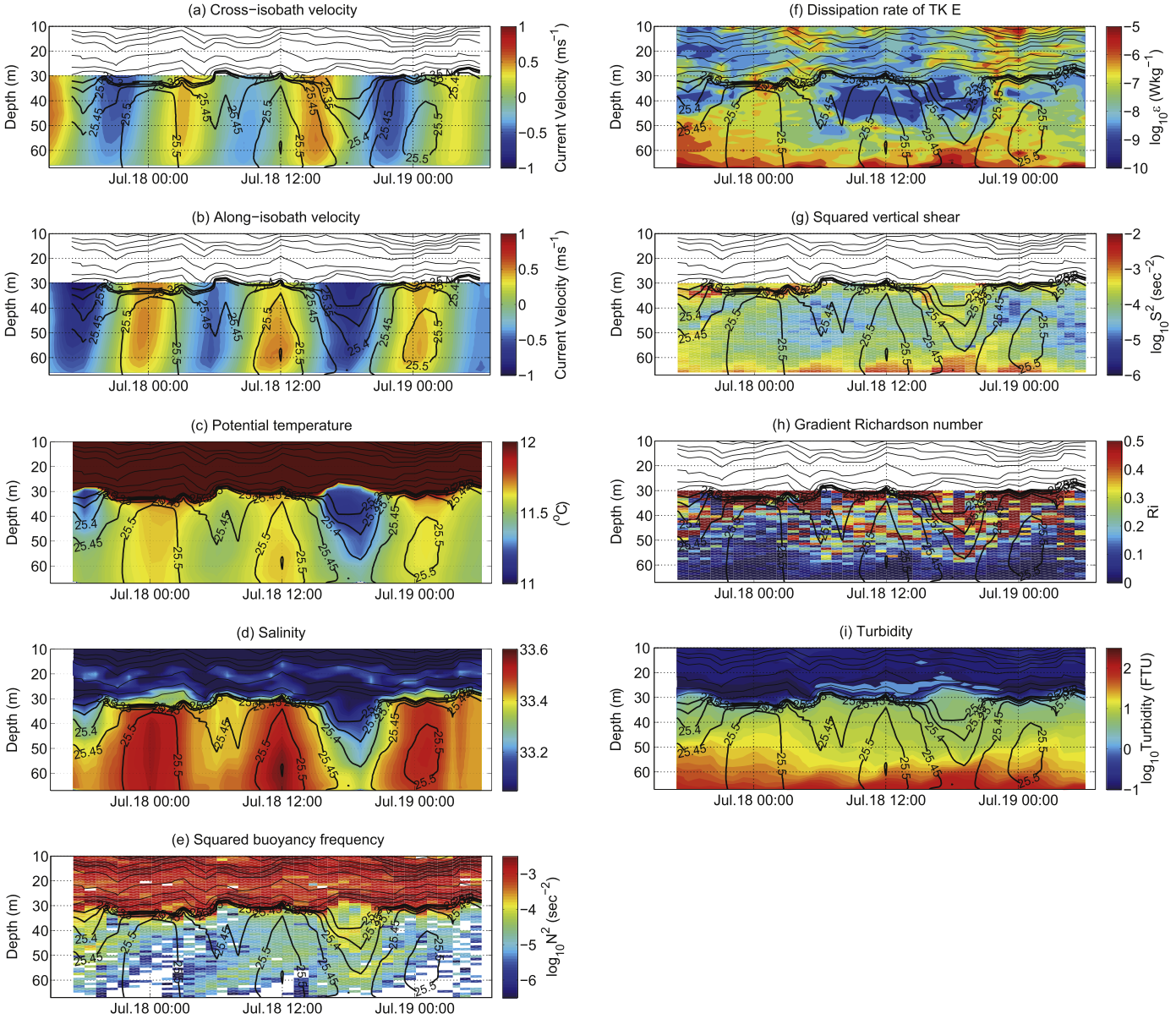

Fig. 2. Time–depth sections of the (a) cross- and (b) along-isobath components of horizontal velocity (U and V), (c) potential temperature, (d) salinity, (e) the squared buoyancy frequency (N^2), (f) the dissipation rate of turbulent kinetic energy (ε), (g) the squared vertical shear of horizontal velocity (S^2), (h) the gradient Richardson number (Ri$=N^2/S^2$), and (i) turbidity, all of which are overlaid with contours of potential density (ρ). The interval between thin (thick) contour lines for potential density less (greater) than $25\sigma_\theta$ is 0.5 (0.05)σ_θ. Note that the ADCP data only in the depth range of 30–65 m are used to draw (a), (b), (g) and (h), where the "percentage of good data" was the maximum value of 100 during the entire period of the observations (i.e. all the single-ping data were judged good). The blank areas in (e) indicate regions of unstable stratification.

of the BBL is that the water column is destabilized during periods of upslope flow (negative U), which is consistent with ShIC (Lorke et al., 2005; Umlauf and Burchard, 2011). In the upper part of the BBL (above a depth of 50 m), a diurnal modulation in the density variations is recognized, the sequence of which is lighter light (at around 1800 JST on July 17), denser dense (at around 0000 JST on July 18), denser light (at around 0600 JST on July 18), lighter dense (at around 1200 JST on July 18), and lighter light (at around 1800 JST on July 18) again. Associated with this, a diurnal modulation in stratification occurs in the upper part of the BBL.

During the period when the upper part of the BBL becomes stratified, strong dissipation ($\varepsilon \geq 10^{-7}$ W kg^{-1}) is confined to the lower part of the BBL (Fig. 2f). By contrast, during the period when stratification in the upper part of the BBL is reduced, high values of dissipation extend throughout the BBL (at around 0000 JST on July 18 and 19). The cycle of dissipation is therefore predominantly diurnal in the upper part of the BBL, corresponding to the variation in N^2 (Fig. 2e), whereas the principal variation in the lower part of the BBL occurs at the quarter-diurnal frequency, corresponding to the variation in S^2 (Fig. 2g). Indeed, enhanced dissipation is seen at depths and during periods where Ri is less than 0.25, the critical value for shear instability (Fig. 2h).

4. Time evolution of potential density

Fig. 2 shows that both the tidal currents and density variations in the BBL are mainly semidiurnal with a noticeable diurnal modulation in the upper part of the BBL. In this section, the relationship between the tidal currents and the time evolution of potential density (ρ) are examined based on the horizontal advection equation:

$$\frac{\partial \rho}{\partial t} = -u\frac{\partial \rho}{\partial x} - v\frac{\partial \rho}{\partial y}, \quad (1)$$

where t is time; and x and y are the eastward and northward coordinates.

We first compare zonal and meridional density gradients ($\partial\rho/\partial x$ and $\partial\rho/\partial y$) estimated using Eq. (1) with those directly calculated from the CTD data, assuming that these gradients are maintained over sub-tidal time scales (several days). By using a least-squares procedure, Eq. (1) is fitted to the time tendency of potential density ($\partial\rho/\partial t$) measured with the TurboMAP-5 and zonal and meridional velocities (u and v) measured with the ADCP. The estimated density gradients agree well with those calculated from the CTD data (Fig. 3a and b) except above a depth of 35 m where the vertical advection of potential density associated with vertical displacements of the pycnocline (Fig. 2) cannot be ignored anymore. In addition, the cross-isobath density gradient ($\partial\rho/\partial n$) shows that potential density in the BBL increases in the downslope direction (Fig. 3c), whereas the along-isobath density gradient ($\partial\rho/\partial s$) is almost zero in the BBL (Fig. 3d). These results indicate that the density variations observed in the BBL result mainly from cross-isobath advection.

As mentioned in the introduction, a direct influence of freshwater is unlikely in the BBL at the observation site, suggesting that

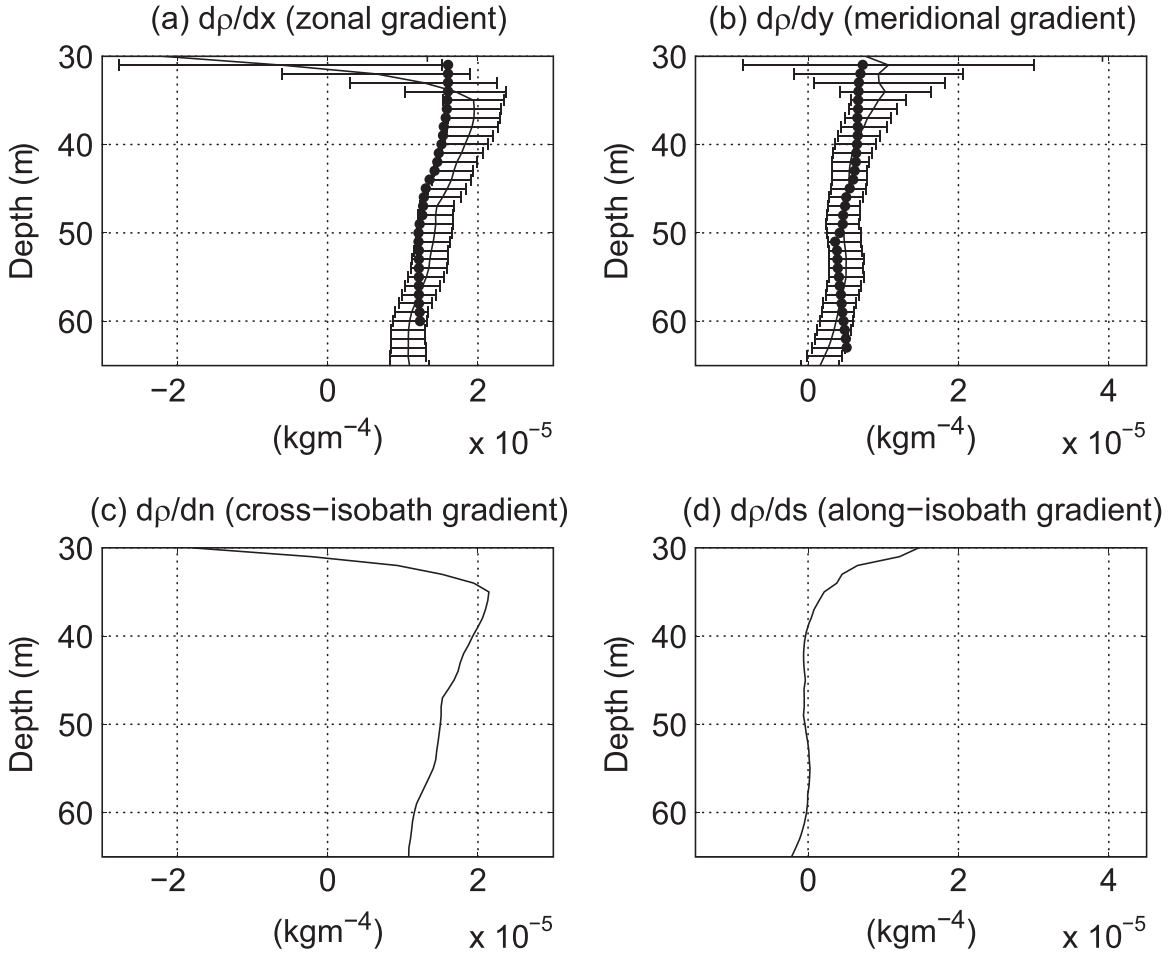

Fig. 3. Vertical profiles of (a) zonal, (b) meridional, (c) cross-isobath, and (d) along-isobath gradients of potential density ($\partial\rho/\partial x$, $\partial\rho/\partial y$, $\partial\rho/\partial n$, and $\partial\rho/\partial s$) estimated from the TurboMAP-5 and ADCP data using (1) (solid lines). In panels (a) and (b), the errorbars indicate the standard error, and the density gradients directly calculated from the CTD data are overlaid with circles. For the geographical locations of the CTD stations, see Fig. 1b.

the cross-isobath density gradient ($\partial\rho/\partial n$) results from the projection of the interior vertical stratification onto the slope. Assuming a uniform slope with slope angle α, we obtain $\partial\rho/\partial n = -(\rho_0/g)N_\infty{}^2 \sin\alpha$ from the projection of the vertical density gradient. Here, ρ_0 ($=1025$ kg m^{-3}) is the reference density of seawater; and N_∞ is the buoyancy frequency observed in the same depth range as our BBL measurements, however, at some downslope location far enough to be unaffected by the BBL (see Umlauf and Burchard, 2011). Although direct observations at such a location are not available, it seems reasonable to assume that $N_\infty{}^2$ is comparable to, or, because of the greater depth, somewhat smaller than N^2 above the BBL at the observation site. Using the estimates of $\alpha \approx -5\times10^{-4}$ rad (Fig. 1b) and $N_\infty{}^2 \approx 10^{-3.5}-10^{-3}$ s^{-2} (Fig. 2e), we obtain values of $1.7\text{–}5.2\times10^{-5}$ kg m^{-4} for $\partial\rho/\partial n$. The consistency of the estimated value of $\partial\rho/\partial n$ with that shown in Fig. 3c supports our hypothesis that the observed cross-isobath density gradient results from the projection of the interior vertical stratification onto the slope. The important point to note is that the generation of tidally periodic stratification in our example is largely a result of the projected vertical density gradient, different from classical tidal straining which requires an externally imposed horizontal density gradient.

Next, we decompose the horizontal velocities in Eq. (1) into semidiurnal, diurnal, and mean constituents using harmonic analysis. Since the length of the ADCP dataset (about 5 days) is not sufficient to accurately determine all semidiurnal and diurnal constituents, only the tidal constituents of M_2 and K_1 are taken into account as representatives of semidiurnal and diurnal motions, respectively. It should be noted that the diurnal constituent inevitably includes near-inertial motions at the latitude of the

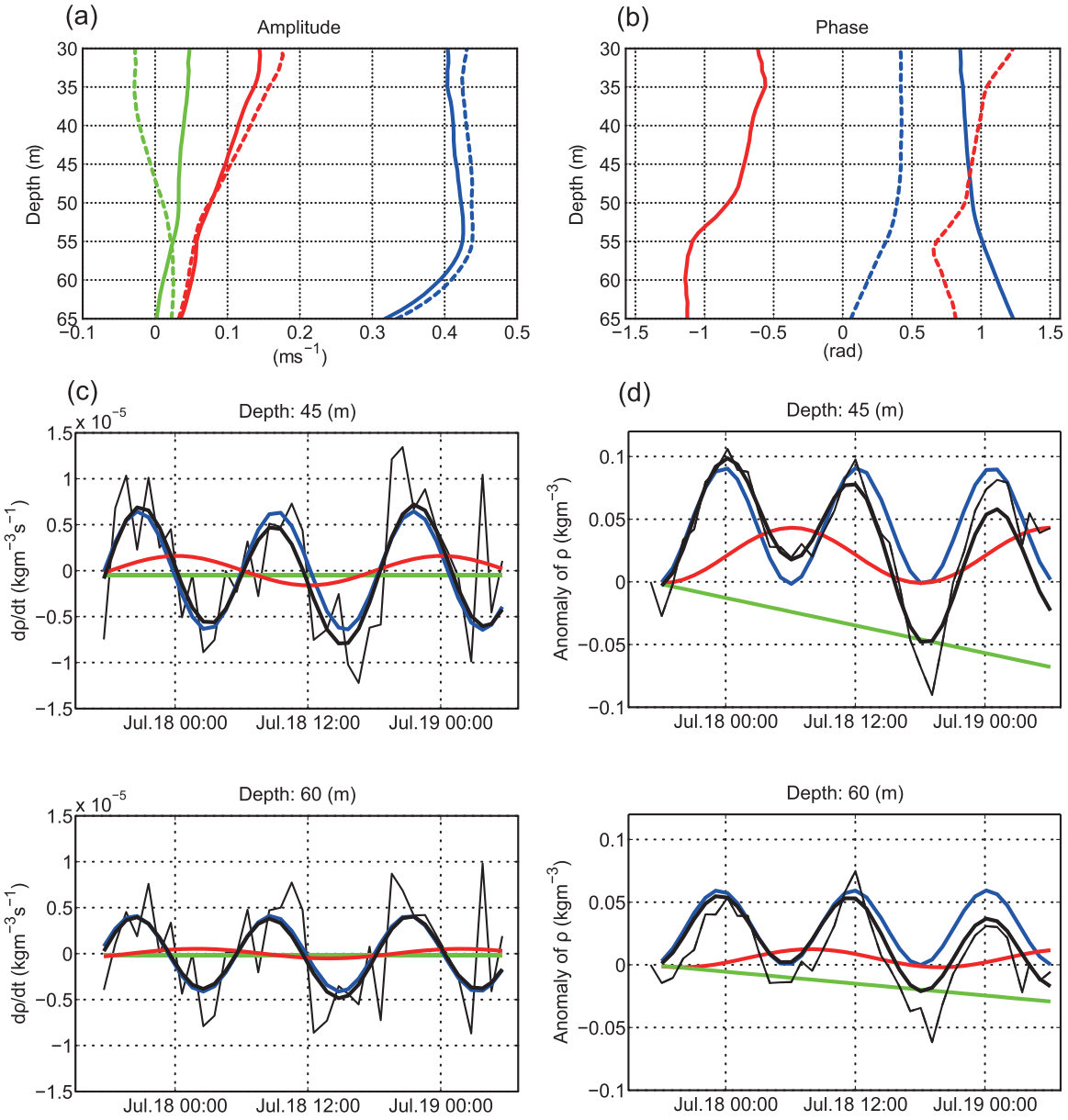

Fig. 4. Vertical profiles of the (a) amplitude and (b) phase of the M_2 (blue lines) and K_1 (red lines) constituents. In panel (a), vertical profiles of the mean component are overlaid with green lines. Solid and dashed lines represent the meridional and zonal components of horizontal velocity, respectively. Time series of (c) the semidiurnal (blue lines), diurnal (red lines), and mean (green lines) components of the horizontal advection term in Eq. (1) and (d) their contributions to density variations at depths of 45 m (upper panels) and 60 m (lower panels). Note that a depth of 50 m is a depth above which the significant diurnal cycle of stratification is observed. Thick black lines in (c) and (d) indicate the sum of all the components and contributions, respectively. Time tendency and anomaly of potential density directly measured with the TurboMAP-5 are overlaid with thin black lines in (c) and (d), respectively. (For interpretation of the references to color in this figure legend, the reader is referred to the web version of this article.)

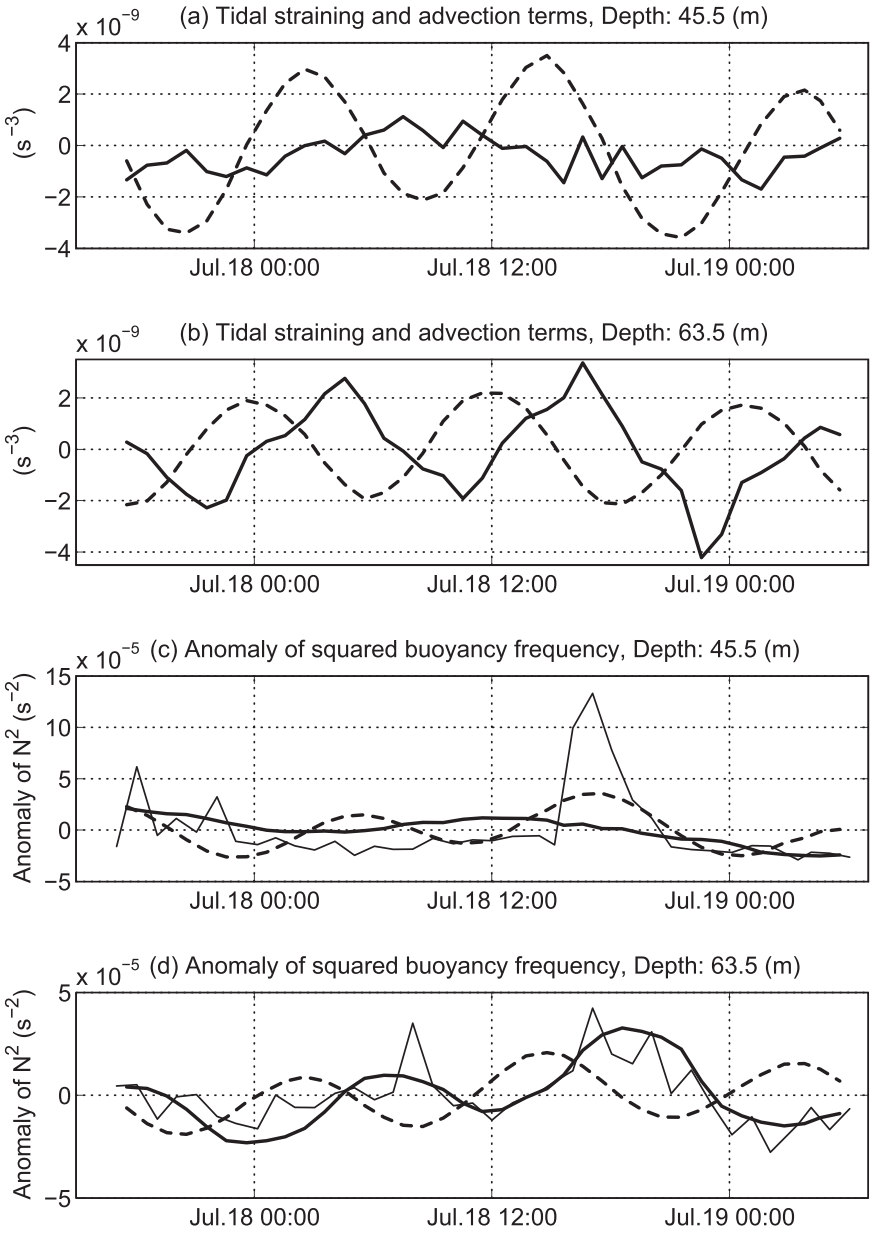

Fig. 5. Time series of the tidal straining (thick solid line) and advection (thick dashed line) terms in Eq. (2) at depths of (a) 45.5 and (b) 63.5 m, as well as those integrated in time and anomaly of the squared buoyancy frequency (N^2) directly measured with the TurboMAP-5 (thin solid line) at depths of (c) 45.5 and (d) 63.5 m.

observation site. As our focus here is on the effect of these quasi-diurnal motions, rather than their cause, this complication does not interfere with our analysis or conclusions. Fig. 4 shows that the amplitude of the M_2 constituent is about four (ten) times larger than that of the K_1 (mean) constituent. For each tidal constituent, the zonal and meridional components have nearly identical amplitudes so that the tidal ellipse has a nearly circular shape. Both the amplitude and phase of the M_2 constituent are uniform above a depth of 50 m. In contrast, the amplitude of the K_1 constituent increases almost linearly with height above the seabed, whereas the phase of the K_1 constituent are nearly uniform above a depth of 50 m. These results are qualitatively consistent with bottom Ekman layer dynamics (e.g. Prandle, 1982; Yoshikawa et al., 2010), since the present observations were carried out at the latitude where the thickness of the bottom Ekman layer for the diurnal motion is much greater than that for the semidiurnal one.

The horizontal velocities decomposed in this way are multiplied by the zonal and meridional density gradients estimated by the least-squares procedure (Fig. 3) to obtain the semidiurnal, diurnal, and mean components of the advection terms in Eq. (1) (Fig. 4c). Each component of the advection terms is then integrated in time to determine contribution to the observed density variations (Fig. 4d). The sum of all the components of the advection terms and the sum of all the contributions (thick black lines) agree well with the time tendency and anomaly of potential density directly measured with the TurboMAP-5 (thin black lines), respectively, both of which are dominated by the semidiurnal components (blue lines). The mean component of the advection terms contributes to a decreasing trend in potential density at both depths (green lines). It should be noted that the remarkable diurnal modulation in potential density is seen only in the upper part of the BBL where the diurnal component of the advection terms is significant (red lines). This can be easily understood from the difference in the amplitudes of the K_1 constituent (Fig. 4a): e.g., the amplitude at the depth of 45 m is twice as large as that at the depth of 60 m. Consequently, the diurnal cycle of potential

density appears only in the upper part of the BBL, as shown in Fig. 2.

5. Time evolution of stratification

Fig. 2 shows a semidiurnal switching between unstable and stable stratification in the lower part of the BBL. The water column is destabilized during periods of upslope flow, which is consistent with ShIC (Lorke et al., 2005; Umlauf and Burchard, 2011). In this section, we investigate the time evolution of stratification by taking the vertical derivative of the horizontal advection Eq. (1), such that

$$\frac{\partial N^2}{\partial t} = \frac{g}{\rho_0}\left(\frac{\partial u}{\partial z}\frac{\partial \rho}{\partial x} + \frac{\partial v}{\partial z}\frac{\partial \rho}{\partial y}\right) + \left(-u\frac{\partial N^2}{\partial x} - v\frac{\partial N^2}{\partial y}\right), \quad (2)$$

where z is a vertical coordinate positive upward. On the right-hand side of Eq. (2), the terms in the first brackets represent tidal straining of horizontal density gradients, whereas the terms in the second brackets represent the advection of existing stratification (Giddings et al., 2011). Both terms are calculated from the horizontal velocities measured with the ADCP and the zonal and meridional density gradients estimated by the least-squares procedure in Section 4.

Although the time evolution of potential density is well described by Eq. (1) (Figs. 3 and 4), the same is not true for Eq. (2). Actually, the sum of the tidal straining and advection terms does not agree very well with the time tendency of N^2 directly measured with the TurboMAP-5 (not shown). One reason for this disagreement is that the vertical derivative is sensitive to the observation error, and another reason is that vertical derivatives of the vertical mixing and advection terms ignored in Eq. (1) are likely to be significant, especially in the lower part of the BBL, where mixing is a first-order effect. Therefore, we discuss here the correlations of the time evolution of stratification with the tidal straining and advection terms integrated in time, instead of the term balance in Eq. (2). In the lower part of the BBL, where the tidal straining term is significant (Fig. 5b), the time-integrated tidal straining term is highly correlated with the observed N^2 (Fig. 5d): the correlation coefficient $r=0.86$, which is statistically significant at the 99% confidence level. Although the tidal advection term is comparable to the tidal straining term, there is no statistically significant correlation between the time-integrated tidal advection term and the observed N^2. In the upper part of the BBL, where the tidal straining term is almost zero (Fig. 5a), there is a moderate correlation ($r=0.64$) between the time-integrated tidal advection term and the observed N^2 (Fig. 5c). These results indicate that semidiurnal switching between unstable and stable stratification in the lower part of the BBL is caused by ShIC, whereas tidal advection of existing stratification dominates the time evolution of stratification in the upper part of the BBL.

6. Concluding remarks

In the present study, we have shown evidence for the existence of tidal straining over sloping topography outside any ROFI, by analyzing a 37-h series of simultaneous measurements of the dissipation rate of turbulent kinetic energy, temperature, salinity, and horizontal velocity over the continental shelf of the ECS. The observations were carried out at about 400 km to the east-northeast of the mouth of the Changjiang River, suggesting that horizontal density gradients maintained by river runoff are negligible in the near-bottom region.

In the lower part of the BBL, the tidal current shear interacting with the cross-isobath density gradient results in semidiurnal strain-induced switching between unstable and stable stratification (Fig. 2e). The cycle of turbulent dissipation is quarter-diurnal, corresponding to the semidiurnal variation of tidal current shear. Most importantly, the observed cross-isobath density gradient triggering the tidal straining process is consistent with the cross-isobath projection of the interior vertical density gradient without taking into account any horizontal density gradients due to river runoff or differential heating (Umlauf and Burchard, 2011). The observed strain-induced switching is therefore likely to be a generally relevant phenomenon on the continental shelf, with possibly important implications for the energetics of tidal mixing, nutrient supply, sediment transport, and other near-bottom processes. In the upper part of the BBL, a noticeable diurnal modulation in stratification as well as a significant diurnal cycle of turbulent dissipation are evident. There, the time evolution of stratification is dominated by tidal advection of existing stratification, rather than tidal straining of horizontal density gradients.

Several important problems still remain to be investigated. First, the spatial distribution of regions of intense tidal straining should be clarified. As mentioned in the introduction, the ECS is known as one of the regions of intense primary productivity. A clear correlation between turbidity originating at the seabed and turbulent dissipation especially in the lower part of the BBL (Fig. 2f and i) suggests that tidal straining might affect the transport of suspended material and hence the biogeochemical cycles in the wide areas of the ECS. For example, a recent modeling study by Schulz and Umlauf (submitted) suggests that tidal straining near sloping topography induces a residual cross-isobath transport of suspended material, similar to the tidal pumping mechanism described in the context of classical tidal straining in estuaries (Jay and Musiak, 1994; Scully and Friedrichs, 2007). Moreover, if the tidal current shear is controlled by bottom Ekman layer dynamics, as suggested in the present study, the influence of tidal straining on stratification and turbulence might vary depending on latitude. Further observations at different locations are required to resolve these issues. Observations over time periods long enough to distinguish the tides from the near-inertial oscillation, as well as measurements of the Reynolds stress, which can be combined with the vertical shear to estimate the turbulent eddy viscosity, are highly desirable. Second, a dynamical link between stratification and turbulent mixing should be investigated in detail. We are currently carrying out detailed numerical studies based on a one-dimensional numerical model that incorporates a turbulence closure scheme as well as a large eddy simulation that takes the observed density gradients and tidal currents into account. Results of these investigations will be reported elsewhere.

Acknowledgment

The authors would like to express their gratitude to the captain and the officers and crew of T/S *Nagasaki-Maru* of the Faculty of Fisheries, Nagasaki University, and the scientific parties on board for their great help in collecting the data. This work was supported through a Grant-in-Aid for Scientific Research provided to T. Endoh, Y. Yoshikawa, Y. Wakata, and T. Matsuno by the Ministry of Education, Culture, Sports, Science and Technology (MEXT) of Japan (22340140 and 26241009), as well as by the Collaborative Research Program of Research Institute for Applied Mechanics (RIAM), Kyushu University. L. Umlauf is grateful for the support by the German Research Foundation (DFG) through grant UM79/6-1.

References

Beardsley, R.C., Limeburner, R., Yu, H., Cannon, G.A., 1985. Discharge of the

Changjiang (Yangtze River) into the East China Sea. Cont. Shelf Res. 4 (1–2), 57–76.
Becherer, J., Umlauf, L., 2011. Boundary mixing in lakes. 1. Modeling the effect of shear-induced convection. J. Geophys. Res. 116, C10017. http://dx.doi.org/10.1029/2011JC 007119.
Becherer, J., Stacey, M.T., Umlauf, L., Burchard, H., 2015. Lateral circulation generates flood tide stratification and estuarine exchange flow in a curved tidal inlet. J. Phys. Oceanogr. 45 (3), 638–656.
Endoh, T., Matsuno, T., Yoshikawa, Y., Tsutsumi, E., 2014. Estimates of the turbulent kinetic energy budget in the oceanic convective boundary layer. J. Oceanogr. 70 (1), 81–90.
Endoh, T., Matsuno, T., Yoshikawa, Y., Tatsuyama, Y., Ishizaka, J., 2009. Observations of wind-driven deepening of the surface mixing layer in the Tsushima Strait. J. Oceanogr. 65 (2), 273–279.
Fisher, N.R., Simpson, J.H., Howarth, M.J., 2002. Turbulent dissipation in the Rhine ROFI forced by tidal flow and wind stress. J. Sea Res. 48, 249–258.
Giddings, S.N., Fong, D.A., Monismith, S.G., 2011. Role of straining and advection in the intratidal evolution of stratification, vertical mixing, and longitudinal dispersion of a shallow, macrotidal, salt wedge estuary. J. Geophys. Res. 116, C03003. http://dx.doi.org/10.1029/2010JC006482.
Jay, D.A., Musiak, J.D., 1994. Particle trapping in estuarine tidal flows. J. Geophys. Res. 99 (C10), 20445–20461.
Larsen, L.H., Cannon, G.A., Choi, B.H., 1985. East China Sea tide currents. Cont. Shelf Res. 4 (1–2), 77–103.
Lorke, A., Peters, F., Wüest, A., 2005. Shear-induced convective mixing in bottom boundary layers on slopes. Limnol. Oceanogr. 50 (5), 1612–1619.
Lorke, A., Umlauf, L., Mohrholz, V., 2008. Stratification and mixing on sloping boundaries. Geophys. Res. Lett. 35, L14610. http://dx.doi.org/10.1029/2008GL034607.
Lu, Y., Lueck, R.G., 1999. Using a broadband ADCP in a tidal channel. part II: turbulence. J. Atmos. Ocean. Technol. 16 (11), 1568–1579.
Nepf, H.M., Geyer, W.R., 1996. Intratidal variations in stratification and mixing in the Hudson estuary. J. Geophys. Res. 101 (C5), 12079–12086.
Prandle, D., 1982. The vertical structure of tidal currents. Geophys. Astrophys. Fluid Dyn. 22, 29–49.
Rippeth, T.P., Fisher, N.R., Simpson, J.H., 2001. The cycle of turbulent dissipation in the presence of tidal straining. J. Phys. Oceanogr. 31 (8), 2458–2471.
Schulz, K., Umlauf, L., submitted. Residual transport of suspended material by tidal straining near sloping topography, J. Phys. Oceanogr.
Scully, M.E., Friedrichs, C.T., 2007. Sediment pumping by tidal asymmetry in a partially mixed estuary. J. Geophys. Res. 112, C07028. http://dx.doi.org/10.1029:/2006JC003784.
Simpson, J.H., 1997. Physical processes in the ROFI regime. J. Mar. Syst. 12 (1–4), 3–15.
Simpson, J.H., Souza, A.J., 1995. Semidiurnal switching of stratification in the region of freshwater influence of Rhine. J. Geophys. Res. 100 (C4), 7037–7044.
Simpson, J.H., Brown, J., Matthews, J., Allen, G., 1990. Tidal straining, density currents, and stirring in the control of estuarine stratification. Estuaries 13 (2), 125–132.
Stacey, M.T., Monismith, S.G., Burau, J.R., 1999a. Observations of turbulence in a partially stratified estuary. J. Phys. Oceanogr. 29 (8), 1950–1970.
Stacey, M.T., Monismith, S.G., Burau, J.R., 1999b. Measurements of Reynolds stress profiles in unstratified tidal flow. J. Geophys. Res. 104 (C5), 10,933–10,949.
Umlauf, L., Burchard, H., 2011. Diapycnal transport and mixing efficiency in stratified boundary layers near sloping topography. J. Phys. Oceanogr. 41 (2), 329–345.
Wolk, F., Yamazaki, H., Seuront, L., Lueck, R.G., 2002. A new free-fall profiler for measuring biophysical microstructure. J. Atmos. Ocean. Technol. 19 (5), 780–793.
Yoshikawa, Y., Endoh, T., Matsuno, T., Wagawa, T., Tsutsumi, E., Yoshimura, H., Morii, Y., 2010. Turbulent bottom Ekman boundary layer measured over a continental shelf. Geophys. Res. Lett. 37, L15605. http://dx.doi.org/10.1029/2010GL044156.
Yoshikawa, Y., Matsuno, T., Wagawa, T., Hasegawa, T., Nishiuchi, K., Okamura, K., Yoshimura, H., Morii, Y., 2012. Tidal and low-frequency currents along the CK line (31°45 min N) over the East China Sea shelf. Cont. Shelf Res. 50–51, 41–53.